LAWRENCE
LIVERMORE
NATIONAL
LABORATORY

UCRL-PROC-20407

Measuring the ionization balance of gold in a low-density plasma of importance to ICF

M.J.May, P.Beiersdorfer, M.Schneider, S.Terracol, K.L.Wong, K.Fournier, B.Wilson, J.H.Scofield, K.J.Reed, G.Brown, F.S.Porter, R.Kelley, C.A.Kilbourne and K.R.Boyce

May 10, 2004

The 14th APS Topical Conference on Atomic Processes in Plasmas, Santa Fe, New Mexico April 19-22, 2004.

Measuring the ionization balance of gold in a low-density plasma of importance to ICF

M.J. May*, P. Beiersdorfer*, M. Schneider*, S. Terracol*, K.L. Wong*, K. Fournier*, B. Wilson*, J.H. Scofield*, K.J. Reed*, G. Brown†, F.S. Porter**, R. Kelley**, C.A. Kilbourne** and K.R. Boyce**

*Lawrence Livermore National Laboratory, L-260, Livermore, CA 94550
†Department of Astronomy, University of Maryland, College Park, MD 20724
**NASA-Goddard Space Flight Center, Code 662, Greenbelt, MD 20700

Abstract. Charge state distributions (CSDs) have been determined in low density ($\approx 10^{12}$ cm^{-3}) gold plasmas having either a monoenergetic beam (E_{Beam} = 2.66, 3.53 and 4.54 keV) or experimentally simulated thermal electron distributions (T_e = 2.0, 2.5 and 3.0 keV). These plasmas were created in the Livermore electron beam ion traps EBIT-I and EBIT-II. Line emission and radiative recombination features of Ni to Kr-like gold ions were recorded in the x-ray region with a crystal spectrometer and a photometrically calibrated microcalorimeter. The CSDs in the experimentally simulated thermal plasmas were inferred by fitting the observed 4f→3d and 5f→3d lines with synthetic spectra from the Hebrew University Lawrence Livermore Atomic Code (HULLAC). Additionally, the CSDs in the beam plasmas were inferred both from fitting the line emission and fitting the radiative recombination emission to calculations from the General Relativistic Atomic Structure Program (GRASP). Despite the relatively simple atomic physics in the low density plasma, differences existed between the experimental CSDs and the simulations from several available codes (e.g. RIGEL). Our experimental CSD relied upon accurate electron impact cross sections provided by HULLAC. To determine their reliability, we have experimentally determined the cross sections for several of the n=3→4 and n=3→5 excitations in Ni to Ga-like Au and compared them to distorted wave calculations. Recent Au spectra recorded during experiments at the HELEN laser facility are presented and compared with those from EBIT-I and EBIT-II.

INTRODUCTION

Predicting the correct charge state distribution (CSD) is critical for understanding radiation levels, energy deposition, energy balance, etc. of high temperature plasmas such as those produced inside Z-pinches [1, 2], tokamaks [3, 4], astrophysical objects [5], and hohlraums irradiated by intense lasers [6, 7]. However, models that calculate CSDs are far from adequate to predict the charge state distribution in a non-local thermodynamic equilibrium (NLTE) plasma. This inadequacy has been strikingly illustrated in a comparison of NLTE calculations of the CSD of several elements [8]. The calculations for high-Z elements at conditions of typical laser-produced plasmas had the most significant discrepancies: for example, the predicted average charge state, $\langle q \rangle$, for gold at a temperature T_e = 2.5 keV and a density $n_e = 10^{20}$ cm^{-3} varied from +43 to +63! The models require several definitive experiments to test their implementation of the atomic physics processes. Such experiments need to be performed at various plasma conditions in order to isolate and study specific atomic physics processes. The low density plasmas

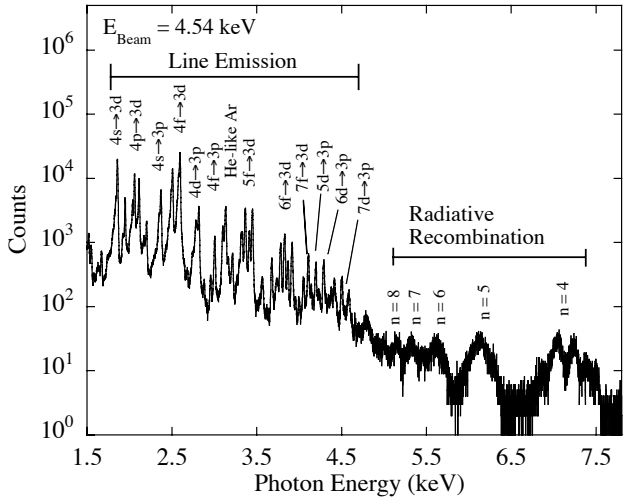

FIGURE 1. Raw XRS spectrum in an EBIT-I plasma having an E_{beam} of 4.54 keV.

have fewer active relevant processes (e.g., no photoionization, opacity, three-body recombination, etc.) and also provide less complicated experiments than the high density ones. One such atomic physics process that can be measured in the low density plasma is electron collisional impact excitation. Errors in these excitation cross sections will alter the CSD inferred by fitting synthetic spectra derived from these cross sections to the measured spectra. Therefore, accurate measurements of the cross sections are necessary. Additionally, calibrated and identified spectra from the low density plasma can significantly aid in the analysis of spectra from the high density laser produced plasma.

Recently, two high density experiments with different plasmas conditions have been done with the NOVA laser to determine the ionization balance of Au. Foord et al. [9] inferred the charge state balance of a heated gold microdot buried in a Be foil at n_e = 6x10^{20} cm^{-3} and T_e = 2.2 keV in steady state by comparing the measured 5f→3d spectrum with atomic physics calculations. The experimental average ionization state, $\langle q \rangle$, = +49.3±0.5 was in reasonable agreement with the modeled value of +49.1 from RIGEL [10]. To reproduce properly the experiment, two-electron processes such as dielectronic recombination (DR) were included in the modeling of the charge balance and the line intensities. Glenzer et al. [11] measured the average gold ion charge state to be +52±1 in a fusion hohlraum plasma with T_e of 2.6 keV, n_e of 1.4x10^{21} cm^{-3}, and a soft x-ray radiation temperature of 210 eV. The predicted steady state $\langle q \rangle$ = +50.5 which was also calculated by RIGEL was just outside the experimental error bar. Glenzer indicated that non-steady state kinetics might be a possible explanation of the discrepancy. The analysis of these high density experiments was complicated by the transient nature of the laser produced plasma and the many competing atomic processes present in these plasmas.

We have inferred CSDs of steady state gold plasmas created in the Livermore electron beam ion traps EBIT-I and EBIT-II.These plasmas had either monoenergetic beams or experimentally simulated thermal electron distributions at electron densities of ≈ 10^{12} cm^{-3}. We recorded the collisionally excited (CE) lines from n=4→3, 5→3, 6→3,

and 7→3 x-ray transitions and radiative recombination (RR) emission from Ni-like to Kr-like gold ions between 1500 and 8000 eV by employing both a photometrically calibrated x-ray microcalorimeter (XRS) [12] and an x-ray crystal spectrometer [13]. These identified and calibrated Au spectra have been used to further the analysis of laser produced plasmas. The CSDs in the beam and the experimentally simulated thermal plasmas were inferred by comparing the x-ray CE line intensities with atomic physics calculations from the Hebrew University Lawrence Livermore Atomic Code (HULLAC) [14]. Additionally, the CSDs in the beam plasmas were inferred by comparisons of the RR features to modeling from the General Relativistic Atomic Structure Program (GRASP) [15, 16]. These measurements observed the ionization balance in steady state conditions. Despite the fewer active processes in the coronal plasma, the inferred CSDs from EBIT-I and EBIT-II disagree with the results from the available modeling codes for both beam and thermal plasmas. The inferred CSDs from spectra recorded in any gold plasma rely upon accurate electron impact cross sections provided by the atomic physics code (e.g. HULLAC). To determine their reliability, we have experimentally determined the cross sections for the 3d→4f and 3d→5f excitations in Ni to Ga-like Au and compared them to theory.

PLASMAS AT THE LIVERMORE ELECTRON BEAM ION TRAPS

Gold plasmas were created in EBIT-I and EBIT-II by successive electron collisional ionization of low-charged ions introduced into the trap from a metal vacuum vapor ion source [17]. Radial trapping of the ions in the electron mode [18] was achieved by the electrostatic attraction of the electron beam. Two end drift tubes, which have a positive bias of a few hundred volts with respect to a center drift tube, confined the ions axially along the beam. Plasmas having either a monoenergetic electron beam or an experimentally simulated thermal electron distribution were utilized to obtain the data presented here. Details of the experiments can be found in Ref. [19, 20].

The monoenergetic electron beam plasmas created in EBIT-I and EBIT-II had energies, E_{beam}, of 2.66, 3.53 and 4.54±0.04 keV. The reported beam energies are corrected for the space charge effects of a beam current of ≈ 55 mA [21]. The electron beam had a Gaussian electron energy distribution with a full width half maximum of ≈ 50 eV. The plasmas with experimentally simulated thermal electron distributions had temperatures, T_e, of 2.0, 2.5 and 3.0±0.04 keV. To create these plasmas, the electron beam energy and anode voltages were swept to map out a Maxwell-Boltzmann (MB) electron distribution in time by using the techniques described in Ref. [22]. In each sweep, the time spent at an electron beam energy was proportional to the experimentally simulated temperature's MB electron distribution probability at that energy. The reported temperatures include the space charge corrections. The beam energy was swept between electron energies of a few hundred eV to 6 or 8 times the temperature of the plasma. With these voltages the majority of the MB distribution was sampled. Concurrently, the anode voltage was swept to maintain a constant density in the electron beam. Each sweep, which lasted 5 ms, was continuously repeated until the end of the trapping cycle. The spectra presented here for both types of plasmas were taken during the steady state portion of the trapping cycle.

This was ≈ 1 s after the start of the studied beam energy or MB sweeps and lasted for 8 to 12 s before the trap was emptied. Each experimental condition required repeating the trapping cycle at the same conditions for ≈12 hrs to record sufficient signal on the spectrometers.

The x-ray crystal spectrometer recorded in first order the high-resolution spectra of the 5f→3d and the 4f→3d transitions of Ni-like to Kr-like gold ions between photon energies of 3100 to 3500 eV and 2400 to 2600 eV, respectively. For these measurements, two Si(111) crystals with lattice spacings of 2d = 6.2712 Å were used. The gas counter detectors were filled with ≈ 1 atm of P10 gas and had either a 4 μm of polypropylene or 1 μm of polyimide window. In addition, each window was coated with a 100 - 200 Å Al layer. A vacuum isolation window composed of 0.5 μm of polyimide was located between the crystal spectrometer and EBIT-I and EBIT-II. The energy resolution was ≈ 5.0 eV at 3300 eV and ≈ 2.5 eV at 2500 eV. The absorption of the gas including the Ar K edge at 3210 eV and the transmission efficiency of the windows were taken into account when the experimental spectrum was compared with the modeling.

The XRS microcalorimeter recorded gold CE lines between 1.5 to ≈ 5.0 keV and RR features from ≈ 5.0 to 8.0 keV. A sample raw spectrum is shown in figure 1 for a plasma having E_{beam} = 4.54. The XRS detector head consisted of an array of ion-implanted thermistors with a 8.5 μm thick HgTe photon absorber. The thermistors directly measured the temperature change of a single photon absorbed by the HgTe. To measure the small changes in temperature, the detector head was cooled to an operating temperature of 59 mK by an adiabatic demagnitization refrigerator mounted inside a Dewar filled with super-fluid helium. Since each absorber-thermistor must be recooled after each photon event, the maximum count rate was limited to ≈ 100 counts per second across the entire array. This count rate is well suited for astrophysical observations and the typical low photon fluxes from EBIT-I and EBIT-II. Two XRS detector front end assemblies have been used at the Livermore EBITs. The first array read out 30 active pixels and had a spectral resolution of ≈ 12 eV. The current version reads out 16 pixels and has a resolution of ≈ 6 eV.

MODELING

The HULLAC [14] atomic data package was used to calculate the atomic structure, transition rates, and synthetic line intensities for the Ni-like to Kr-like Au ions. The radiative transition rates and energy level structure of each ionization state were calculated from the Dirac equation with a parametric potential. Electron impact excitation cross sections, σ_{CE}, were calculated semi-relativistically in the distorted wave approximation. Details of the CE modeling are discussed in Refs. [19, 20].

Due to the low electron density of the trapped ions, the modeling only addresses transitions that are fed primarily through collisional excitation from the ground level. Nevertheless, all possible n=4→4 and n=3→4 to 3→7 excitations to singly excited configurations were included for Ni to Ga-like ions. The models for the Ge to Kr-like ions contained only the n=4→4, n=3→4 and 3→5 excitations. The simpler ions such as Ni and Kr-like gold included several hundred levels. The more complicated ions such as

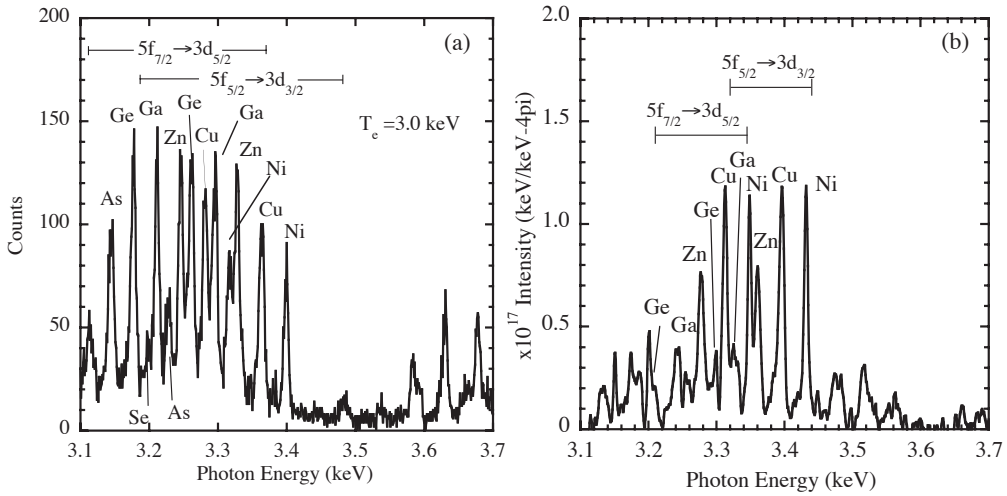

FIGURE 2. (a) Au spectrum from an EBIT-I plasma having T_e of 3.0 keV recorded by the XRS microcalorimeter which required $\approx$ 12 hours of data acquisition. (b) Spectrum from a gold foil taken at AWE. Line identifications were done by comparisons with the spectrum in (a)

As-like gold had several thousand levels. When just the line intensities were desired, the level populations of each ionization state were coupled with only the adjacent, higher-charged ion. The model for the higher-charged ion included fewer levels than the lower-charged ion and was only considered to include the small effect of dielectronic recombination on the collisionally excited transitions. Dielectronic recombination rate coefficients were found by requiring detailed balance of the HULLAC autoionization rates. When a CSD was computed, all the charge state models from Ni-like to Kr-like were coupled together and run until a steady state solution was reached. These models were small and did not include all the high-n transitions and were not used for the spectral analysis.

The rate coefficients and the radiative transition probabilities were put into a collisional-radiative matrix. The level populations were calculated by solving the coupled set of equations:

$$\frac{dn_j}{dt} = 0 = \sum_i n_i R_{i\rightarrow j} - n_j \sum_i R_{j\rightarrow i}$$

where n_i is the relative population of level 'i' of a given ion, $R_{j\rightarrow i}$ is the rate at which population transfers from level 'j' to level 'i' which can be in the adjacent ionization state. All electric and magnetic dipole and quadrupole radiative transitions and relevant magnetic octopole transitions were included. In the EBIT-I and EBIT-II plasmas, collisional electron excitation from the ground level or metastable levels was the only significant process to populate an upper level. The effect of the metastable populations was included in the calculations.

Synthetic spectra were produced for detailed comparisons and fitting to the XRS and crystal spectra from both the monoenergetic beam plasmas and thermal plasmas. The relative emissivity, $J_{i\rightarrow j}$, for each transition within an ionization state was calculated for

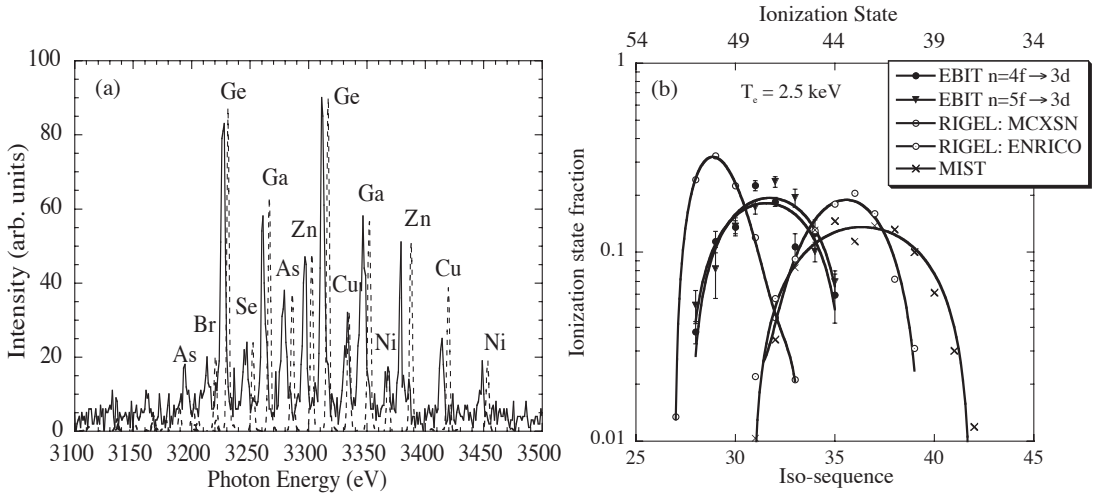

FIGURE 3. (a) Gold emission spectrum produced by a 2.5 keV experimentally simulated Maxwell-Boltzmann temperature. Dashed lines are the HULLAC fits which are used to infer the CSD. (b) Comparison of the gold CSD at 2.5 keV determined from EBIT-II to the results from RIGEL/MCXSN, RIGEL/ENRICO and MIST. The lines are only added to guide the eye. The dip at Kr-like ion in the MIST charge balance is due to the inclusion of the excitation-autoionization rates of Mitnik et. al. [27] missing in the lower charge states.

either a MB temperature or a Gaussian electron distribution with ΔE_{FWHM} =50 eV at n_e = 1x10^{12} cm^{-3}.

GRASP [15] simulated the RR features for comparison with the spectra recorded by the XRS from the beam plasmas. GRASP is an atomic structure code that determined the bound state radial wave functions by numerically solving the multiconfiguration Dirac-Fock functions. Modifications of the code [16] produce the matrix elements and the cross sections for the continuum processes of RR and dielectronic recombination. GRASP provides cross sections that account for the polarization effects in our EBITs.

COMPARISON WITH LASER PLASMAS

Spectra from laser produced plasmas can be very complicated with many competing processes contributing to the line intensities (e.g. opacity, three-body recombination, etc). The basic identification of a transition and its corresponding charge state can be very challenging. Accurate photon energy measurements and line identifications in the spectra taken at EBIT-I and EBIT-II can significantly aid in this analysis. In addition, the measured line intensities in can be directly compared to the laser produce plasma spectra.

In EBIT-I and EBIT-II plasmas, the beam energy is user selectable allowing a specific set of gold ionization states to be isolated in the trap for analysis. For instance, the E_{beam} = 4.54 keV plasma (figure 1) is near the calculated ionization threshold of Ni-like gold at 4.89 keV but well above the threshold to ionize Cu-like into Ni-like at 2.96 keV. Therefore, Ni-like Au was the dominant ion in the trap and produced the most intense emission lines. The Cu-like and Zn-like ions existed in the trap but in

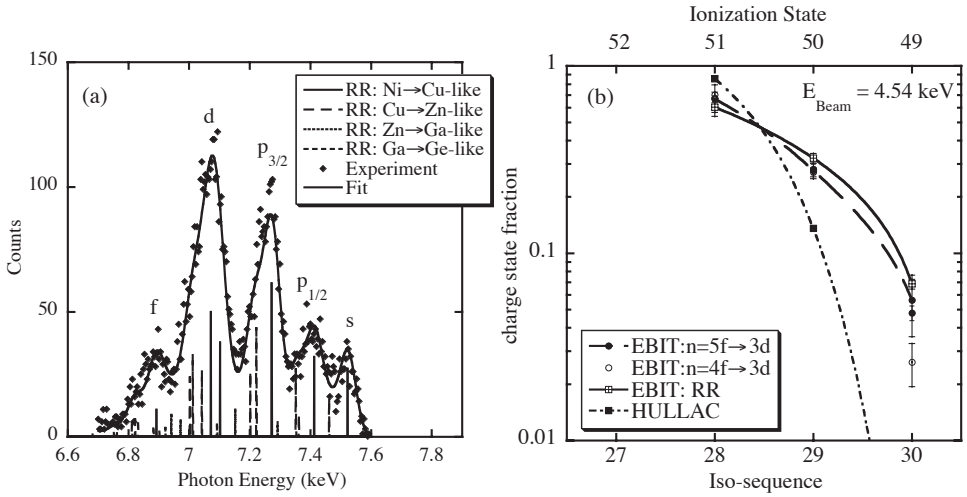

FIGURE 4. (a) Radiative recombination spectrum measured by the XRS in a plasma with an E_{Beam} = 4.54 keV. The RR features are fit with calculations from GRASP to infer the CSD. (b) CSD inferred from both the 5f→3d, 4f→3d and fitting with HULLAC calculations and the RR spectrum and fitting with GRASP calculations. The experimentally inferred CSDs are self consistent but differ from that determined by HULLAC.

smaller concentrations and produced weaker line emission. By appropriately adjusting the beam energy, the charge distribution in the trap was shifted to ions as low as Kr-like. Unambiguous line identifications and accurate photon energy measurements were done for many collisionally excited transitions through comparisons with HULLAC modeling. Approximately 140 lines have been identified in the 9 charge states. The uncertainty in the photon energies was $\approx$ 0.5 eV using the crystal spectrometer.

A spectrum of the 5f→3d transitions from a simulated thermal plasma with T_e = 3.0 keV in EBIT-I is shown in figure 2a. This identified and calibrated spectrum was taken with the XRS at a spectral resolution of $\approx$ 6 eV. The same spectrum from a Au foil heated by the HELEN Laser at AWE is shown in figure 2b. A Henway [26] convex crystal spectrometer recorded the spectrum with a similar spectral resolution. The two spectra are very similar. Identification and analysis of the HELEN spectrum was much simplified by direct comparison with the well understood low density spectrum.

CHARGE STATE DISTRIBUTIONS

The CSDs from EBIT-I and EBIT-II plasmas with the experimentally simulated MB electron distributions were determined by individually fitting the intensities of the 5f→3d and 4f→3d emission lines of each charge state with simulated spectra from the HULLAC atomic data package. The 5f→3d and 4f→3d line groups were fit separately. A 5f→3d spectrum from the T_e = 2.5 keV plasma is shown in figure 3a. The HULLAC fits (dashed lines) included the corrections for the spectrometer photometric sensitivity. The resulting experimentally inferred CSD from this plasma is shown in figure 3b. Each point is the ionic fraction derived from the fit of the HULLAC intensities to one or two

lines. The error that brackets each point included the statistical error from the counts in the spectral lines and the uncertainty in the fit to the line or lines in each charge state. The line intensities calculated by HULLAC are assumed not to have any intrinsic error. The experiment is compared with the simulations from the available modeling codes: RIGEL/MCXSN, RIGEL/ENRICO and the Multiple Ionization State Transport (MIST) [24] code. RIGEL is typically used for high-density laser heated plasma experiments and is a superconfiguration-based collisional-radiative code and solves for a CSD by using Monte Carlo techniques. MCXSN generates atomic physics rates for RIGEL based on hydrogenic supershells. ENRICO solves the Dirac equation explicitly to compute the RR and Auger processes. The collisional processes are calculated using generalized formulas. MIST is a low-density (10^{12} to 10^{14} cm^{-3}) tokamak impurity transport code and utilized the average ion model for the basis of its atomic physics rates [25]. Inclusion of the excitation-autoionization rates of Mitnik et. al. [27] in MIST for charge states more highly ionized than Kr-like ions produced the dip in the charge balance at Kr-like Au. The codes have been run with n_e = 1x10^{12} cm^{-3} and T_e = 2.5 keV. The calculations bracket the experiment. The $\langle q \rangle$ was 47.1$\pm$0.4. This is the average from both the n=5$\rightarrow$3 and n=4$\rightarrow$3 spectra. MIST predicted a lower average charge state by 4. RIGEL/MCXSN and RIGEL/ENRICO predicted a higher and lower average charge state by 3. Even by using the better implementation of atomic physics in RIGEL/ENRICO, a better calculation of the CSD is not obtained.

The CSD from the beam plasmas was determined by two separate methods. First, the 5f$\rightarrow$3d and 4f$\rightarrow$3d lines were fit with the HULLAC synthetic spectrum in a manner similar to that described for the thermal plasmas. Second, the RR features were fit with simulations of the RR emission from GRASP. The RR spectrum for a monoenergetic Au plasma at E_{Beam} = 4.54 keV is shown in figure 4. The recombination of Ni$\rightarrow$Cu, Cu$\rightarrow$Zn, Zn$\rightarrow$Ga and Ga$\rightarrow$Ge were seen from the continuum into the n = 4s, $4p_{1/2}$, $4p_{3/2}$, 4d and 4f sublevels. In the beam plasma, the RR features appear as lines with widths equal to the FWHM of the Gaussian electron energy distribution. The energy of the 'line' is equal to the beam energy plus the energy of recombination from the continuum into the final state. The inferred CSDs from both the fits to the RR and the CE emission are shown for this plasma in figure 4b. Both methods of inferring the CSD are very consistent. The $\langle q \rangle$ from the CE lines is 50.6$\pm$0.9 and is consistent with the $\langle q \rangle$ of 50.5$\pm$1.0 from the RR features. The CSD predicted by HULLAC did not agree with experiment. However, the $\langle q \rangle$ of 51.1 was reasonably close.

COLLISIONAL EXCITATIONS CROSS SECTIONS

The CSD from any Au plasma inferred from spectral fitting, directly depends on the accuracy of the electron impact collisional excitation cross sections, σ_{CE}, provided by the atomic structure codes (e.g. HULLAC). To determine the accuracy of the distorted wave calculations, absolute cross section measurements of the 3d$\rightarrow$4f and 3d$\rightarrow$5f excitations in Ni-like to Ga-like Au were done in EBIT-I and EBIT-II. Details of the method can be found in Ref [28]. The total cross sections were determined from the intensities of the CE lines and RR emission recorded by the XRS in the beam plasmas using the formula:

$$\sigma_{CE} = \frac{\sum_j G_j^{RR} \eta_j^{RR} T_j^{RR} \sigma_j^{RR}}{G^{CE} \eta^{CE} T^{CE}} \frac{I^{CE}}{I^{RR}}$$

The sum, j, is over the fine structure levels. The intensities, I, are determined from the fits of the CE and RR features explained above. The variables η and T are the XRS detector efficiency and filter transmissions, respectively. The CE lines and RR features from EBIT-I and EBIT-II plasma are polarized. The polarization, P, is accounted for in the determination of the cross sections. The variable, G, is the angular distribution of the polarization, and G=3/(3-P) for a dipole transition at 90^o. Polarization is a function of the magnetic sublevel cross sections which were calculated using a relativistic distorted wave code (DWS) [29]. For the Ni-like $3d_{3/2} \rightarrow 5f_{5/2}$ excitation having J=1→0, P = (σ_{-1}- $2\sigma_0$+ σ_{+1})/ (σ_{-1}+ $2\sigma_0$+ σ_{+1}). The polarization is ≈ 0.3 at a E_{Beam} = 4.54 keV.

The calculated total cross sections for the Ni-like 3d→4f and 3d→5f excitations are compared with the measured values in figure 5. The theoretical cross sections from HULLAC (dashed lines) are consistent with those from DWS. The points are the measured cross sections. The error bars on each point included the statistical error from the counts in the spectral line and RR features, the uncertainty in the fits to the line or RR features in each charge state, and the uncertainty in the XRS photometric calibration. The $3d_{5/2} \rightarrow 5f_{7/2}$, $3d_{3/2} \rightarrow 5f_{5/2}$ and $3d_{3/2} \rightarrow 4f_{5/2}$ experimental cross sections are in good agreement with the calculations. The experimental cross sections for the $3d_{5/2} \rightarrow 4f_{7/2}$ excitation is ≈ 1.5 times the theory. The measurement demonstrates that some (isolated) errors exist in the calculations of excitation cross sections. However, these were not enough to appreciably change the inferred CSD using HULLAC.

CONCLUSION

Gold CE line and RR emission have been recorded from monoenergetic beam plasmas (E_{Beam}=2.66, 3.53 and 4.54 keV) and simulated thermal plasmas (T_e=2.0, 2.5 and 3.0 keV) created in EBIT-I and EBIT-II . We have unambiguously identified many emission lines of Ni-like to Kr-like Au in the 1.5 to 5 keV x-ray region and have accurate measurements of their photon energies. These calibrated and identified low density gold spectra are very useful in the analysis of gold spectra recorded in laser produced plasmas. The CSDs for the beam plasmas in our EBITs have been determined by fitting CE and the RR spectra with HULLAC synthetic spectra and GRASP RR calculations, respectively. The CSDs for the plasma with the experimentally simulated thermal electron distributions were determined solely from fitting the CE spectra with HULLAC modeling. The experimental CSDs in both types of plasmas are self-consistent. However, the available modeling codes do not adequately reproduce the measurements. The collisional excitation cross sections have been measured for the 3d→4f and 3d→5f excitations in Ni to Ga-like Au . There is reasonable agreement between the measured and calculated cross sections. However, some discrepancies do exist.

This work was performed under the auspices of the U. S. DoE by the University of California Lawrence Livermore National Laboratory under contract W-7405-ENG-48.

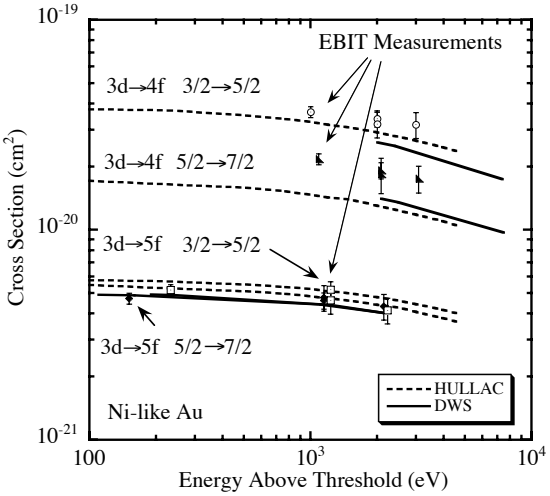

FIGURE 5. Measured collisional excitation cross sections for 3d→4f and 3d→5f transitions in Ni-like Au and comparisons to distorted wave calculations.

REFERENCES

1. K. L. Wong *et al*, Phys. Rev. Lett. **80**, 2334 (1998).
2. A.L. Velikovich *et al*, Physics of Plasmas **8**, 4509 (2001).
3. C. De Michelis and M. Mattioli, Rep. Prog. Phys. **47**, 1233 (1984).
4. J.E. Rice *et al*, J. Phys. B: At. Mol. Opt. Phys. **29**, 2191-2208 (1996).
5. J. C. Raymond and N. C. Brickhouse, Astrophy. and Space Science **237**, 321 (1996).
6. H. R. Griem Phys. Fluids B **4**, 2346 (1992).
7. J. Lindl, Phys. Plasmas **2**, 3933 (1995).
8. R.W. Lee *et al*, J. Quant. Spectrosc., Radiat. Transfer **58**, 737 (1997).
9. M. E. Foord *et al*, Phys. Rev. Lett. **85**, 992 (2000).
10. B. G. Wilson *et al*, Radiative Properties of Hot Dense Matter, edited by W. Goldstein, C. Hooper, J. Gauthier, J. Seely, and R. Lee (World Scientific, Singapore, 1991).
11. S. H. Glenzer *et al*, Phys. Rev. Lett. **87**, 045002 (2001).
12. F. S. Porter *et. al.*, Proc. SPIE **4140**, 407-418 (2000).
13. G. V. Brown *et. al.*, Rev. Sci. Instrum. **70**, 280 (1999).
14. A. Bar-Shalom *et al*, Jour. of Quant. Spect. and Rad. Trans. **71**, 169 (2001).
15. F.A. Parpia *et al*, Comput. Phys. Commun **94**, 249 (1996).
16. J.H. Scofield, Phys. Rev. A, **9**, No. 3, 3054 (1989).
17. I. G. Brown, *et. al.*, Appl. Phys. Lett. **49**, 1019 (1986).
18. P. Beiersdorfer, *et. al.*, Rev. Sci. Instrum. **67**, 3818 (1996).
19. K.L. Wong *et al*, Phys. Rev. Lett. **90**, 235001-1 (2003).
20. M.J. May *et al*, Phys. Rev. E. **68**, 036402 (2003).
21. M. A. Levine *et al*, Phys. Scripta **22**, 157 (1988).
22. D. W. Savin *et. al.*, Rev. Sci. Instrum. **71**, 3362 (2000).
23. R. Marrs *et al*, Phys. Today **47**, 27 (1994).
24. R.A. Hulse Nuclear Technology Fusion **3**, 259 (Mar 1983).
25. D.E. Post *et. al.*, Atomic Data and Nuclear Tables **20**, 397 (1977).
26. L. Koppel and J. Eckels, Lawrence Livermore National Laboratory Report, UCRL-79781 (1977).
27. D. Mitnik *et. al.*, Phys. Rev. A **50**, 4911 (1994).
28. H. Chen *et. al.*, Astrophysical Journal **567**, L169 (2002).
29. H. L. Zhang *et. al.*, Phys. Rev. A 41,198 (1990).